

Customizable Quantum Control via Stimulated Raman User-Defined Passage


Jingjing Niu^{1,2,3,§}, Bao-Jie Liu^{4,§}, Yuxuan Zhou^{1,2,3,4,§}, Tongxing Yan^{1,2,3}, Wenhui Huang^{1,2,3,4},
Weiyang Liu,¹ Libo Zhang,^{1,2,3} Hao Jia,^{1,2,3} Song Liu,^{1,2,3,*} Man-Hong Yung^{1,2,3,†},
Yuanzhen Chen^{1,2,3,4,‡} and Dapeng Yu^{1,2,3,4}

¹*Shenzhen Institute for Quantum Science and Engineering, Southern University of Science and Technology, Shenzhen 518055, China*

²*International Quantum Academy, Shenzhen 518048, China*

³*Guangdong Provincial Key Laboratory of Quantum Science and Engineering, Southern University of Science and Technology, Shenzhen 518055, China*

⁴*Department of Physics, Southern University of Science and Technology, Shenzhen 518055, China*

 (Received 29 November 2021; accepted 21 January 2022; published 23 March 2022)

Adiabatic quantum-control schemes are widely used in the areas of quantum-information processing and quantum sensing. The very requirement of adiabaticity in these schemes often leads to problems of low efficiency and being sensitive to decoherence. To address such issues, various methods have been developed for accelerating adiabatic processes, but they often need to be designed on an *ad hoc* basis. Here we propose and experimentally demonstrate an inverse-engineering approach, where a parameterized state of the Schrödinger equation is employed for constructing desired evolutions. Within a single and simple frame, the user-defined passages can be flexibly customized for different objectives and systems. To experimentally benchmark its performance, we implement this approach in a task of coherent state transfer in a superconducting Xmon device. We find that our method completed the transfer with the fastest speed and highest efficiency (>99.5%) among all recent experiments performed in similar configurations.

DOI: [10.1103/PhysRevApplied.17.034056](https://doi.org/10.1103/PhysRevApplied.17.034056)

I. INTRODUCTION

Quantum processes of an adiabatic nature are widely used in quantum control and quantum sensing. Among the many applications are coherent state transfer [1–4], preparation of quantum states [5–7], as well as dynamic and geometric quantum gates [8–18]. One celebrated example is the stimulated Raman adiabatic passage (STIRAP), originally proposed for coherent population transfer between two uncoupled or weakly coupled quantum states via an intermediate state [1,19,20]. It is immune to the loss through spontaneous emission of the intermediate state, and the adiabaticity guarantees its robustness against fluctuations in control parameters [21]. However, the very requirement of adiabaticity in these schemes leads to two issues. Firstly, the efficiency or fidelity can approach unity only in the long-time limit. Secondly, a slow passage is undesirable since decoherence is ubiquitous.

To address such issues, various approaches have been proposed to accelerate adiabatic processes. These proposals can be roughly categorized into two families named as shortcut to adiabaticity (STA) [22–31] and inverse engineering [32–36]. The original STA methods utilize a counterdiabatic driving to recast adiabatic paths [26–30], which requires a direct coupling between the initial and final states. On the other hand, inverse-engineering methods based on dressed states [33] or dynamical invariants [34] do not require direct coupling. But finding representations of dressed states or constructing proper dynamical invariants may become rather complicated, especially for high-dimensional quantum systems [22].

Alternative methods falling into the category of inverse engineering have thus been developed [37–40]. Instead of searching for proper dressed states or dynamical invariants, these methods set off by parameterizing solutions of the Schrödinger equation that governs the system evolution. Arbitrary control passages connecting the initial and targeted states are realized via carefully engineering the above parameters. These methods have been successfully implemented in two- [37,39] and three-level systems [38,40], as well as nonlinear systems [38,39].

*lius3@sustech.edu.cn

†yung@sustech.edu.cn

‡chenyz@sustech.edu.cn

§These authors contributed equally to this work.

Here we develop a scheme of quantum control via inverse engineering based on the proposal of Ref. [38]. By designing a parameterized solution of the Schrödinger equation of a three-level system, we are able to realize arbitrary passages including both adiabatic and accelerated ones. For example, our scheme automatically becomes STIRAP in the adiabatic limit and realizes accelerated coherent population transfer otherwise. Within the same framework, our method can easily generate customized passages that are optimized for the desired control task and system characteristics such as configuration (e.g., Λ or Ξ configuration) and decoherence.

For an experimental demonstration, the method is applied to realize a coherent population transfer from the state $|0\rangle$ to $|2\rangle$ in an Xmon type of superconducting device. Previously, STIRAP was realized experimentally [3,4,7] with a fidelity of no more than 97%, which is reproduced in our experiment. Recently, STA was also experimentally implemented on a superconducting platform for the same task, with the help of an additional microwave pulse for counterdiabatic driving [30], but only 96% fidelity was achieved. In contrast, both STIRAP and our method require only two microwave pulses to complete the state transfer. Our method can be more than 4 times faster than STIRAP for the same fidelity, and the fidelity can reach >99.5%, after pulse optimization against errors from leakage and cross-coupling.

II. SETTING THE STAGE

Let us consider a three-level system under two external drives with time-dependent amplitudes, $\Omega_P(t)$ and $\Omega_S(t)$, as shown in Fig. 1(a). Under the rotating-wave approximation, the Hamiltonian of this driven system reads $H_0(t) = \frac{1}{2}[\Omega_P(t)|0\rangle\langle 1| + \Omega_S(t)|1\rangle\langle 2| + \text{H.c.}]$. One of its three eigenstates, $|D_0(t)\rangle = \cos\theta(t)|0\rangle - \sin\theta(t)|2\rangle$ [$\tan\theta(t) = \Omega_P(t)/\Omega_S(t)$], is a dark state, which is dynamically decoupled from the system evolution under the adiabatic condition [41]. STIRAP uses this dark state to realize a coherent population transfer from state $|0\rangle$ to $|2\rangle$ by evolving the mixing angle $\theta(t)$, without populating state $|1\rangle$ [41]. In order to keep the system in the dark state, $\theta(t)$ is varied adiabatically to avoid transitions to other eigenstates of $H_0(t)$, which is called ‘‘adiabatic passage.’’

In the following we maintain the setting of STIRAP, but provide a broader perspective on the use of ‘‘passage’’ for quantum control. Specifically, here the concept of passage is extended by defining some time-parameterized state (as input) for inverse engineering the driving Hamiltonian (as output). In this way, one gains higher flexibility in incorporating various optimizations for boosting performance. This strategy can also be applied to other quantum control applications beyond quantum state transfer. To keep our notation simple, in the following we label the user-defined passages used in our study as UDPs.

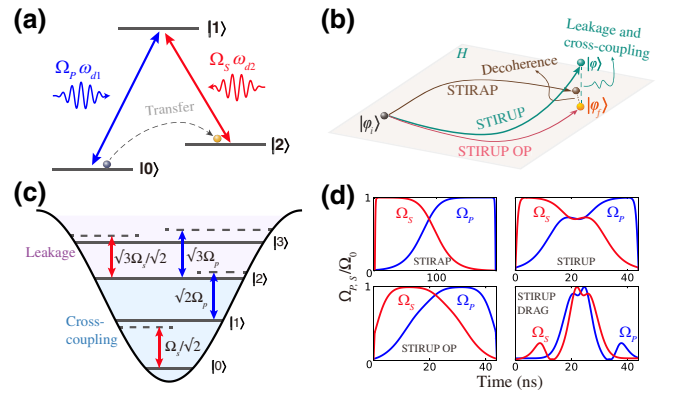


FIG. 1. Concept and implementation of various passage schemes. (a) Multilevel system driven by two external resonant pulses with time-dependent amplitudes. (b) Schematic of different passages. For multilevel systems with non-negligible cross-coupling and leakage, unoptimized UDPs may lead to significant leakage out of the relevant Hilbert space. (c) Cross-coupling and leakage to higher excitations in a multilevel system with weak anharmonicity such as an Xmon type of superconducting device. For example, the Stokes pulse that resonantly couples $|1\rangle$ and $|2\rangle$ in (a) can now also introduce an off-resonant coupling between $|0\rangle$ and $|1\rangle$ in an Xmon. (d) Envelopes of microwave pulses used for the four cases studied in this work: STIRAP, UDP (no optimization), UDP OP, and UDP DRAG (both are optimized, see the main text for details).

For this purpose, the UDPs for a three-level system can be generally parameterized as (up to a global phase):

$$|\Phi_{UD}\rangle = \cos\gamma \cos\beta|0\rangle + e^{i\phi_1} \sin\gamma|1\rangle - e^{i\phi_2} \cos\gamma \sin\beta|2\rangle, \quad (1)$$

where $\beta(t)$, $\gamma(t)$, $\phi_{1,2}(t)$ are generally time-dependent variables to be determined below. To achieve state transfer from $|0\rangle$ to $|2\rangle$, it is sufficient to impose the following boundary conditions: $\gamma(0) = \gamma(T) = 0$, $\beta(0) = 0$, and $\beta(T) = \pi/2$ at time $t = 0$ and $t = T > 0$, respectively. Note that in the adiabatic limit, the state defined by Eq. (1) approaches the dark state in STIRAP and the UDPs thus approach STIRAP (see Appendix B). In addition to STIRAP, our method can also retrieve certain other schemes of coherent control [41,42], such as those based on dressed states [33] and dynamical invariants [34] (see Appendix D).

Consequently, the time dependence of the control pulses can be determined by the passage through the Schrödinger equation,

$$\begin{aligned} \Omega_P &= 2[\dot{\beta} \cot\gamma \sin\beta + \dot{\gamma} \cos\beta]e^{-i\phi}, \\ \Omega_S &= 2[\dot{\beta} \cot\gamma \cos\beta - (\dot{\gamma} - i\dot{\phi}_2 \cot\gamma) \sin\beta]e^{i(\phi_2 - \phi)}, \end{aligned} \quad (2)$$

where $\phi \equiv \phi_1 + \pi/2$. To eliminate the phase factors, we can choose $\phi = 0$ and $\phi_2 = 0$ for simplicity. Note however that extra care must be taken at $t = 0$ and $t = T$, as the boundary conditions would imply a divergence of the driving pulses whenever $\cot \gamma|_{\gamma \rightarrow 0} \rightarrow \infty$.

To overcome such a problem, it is sufficient to maintain the combination $G(t) \equiv \dot{\beta}(t) \cot \gamma(t)$ to be finite. In other words, on the user-defined passage we enforce additional boundary conditions: $G(0) \neq 0$, $G(T) \neq 0$, and $\dot{\beta}(0) \approx \dot{\beta}(T) \approx 0$, where one simple choice for β is found to be $\beta(t) = \pi/21/1 + e^{-10(t/T-1/2)}$. As a result, we rewrite the above relations as follows:

$$\begin{aligned}\Omega_P &= \sqrt{G^2 + \dot{\gamma}^2} \sin[\beta + \arctan(\dot{\gamma}/G)], \\ \Omega_S &= \sqrt{G^2 + \dot{\gamma}^2} \cos[\beta + \arctan(\dot{\gamma}/G)].\end{aligned}\quad (3)$$

To demonstrate the flexibility, we provide three options (i) choose $G(t) = \Omega_0$ to be some constant. (ii) To reduce the population of intermediate level $|1\rangle$ [$P_1(t) = |\sin \gamma(t)|^2$], we can instead choose the parameter as $G(t) = \Omega_0[1 + Ae^{-(t/T-1/2)^2/B^2}]$ to reduce $\gamma(t) = \arctan[\dot{\beta}(t)/G(t)]$, where A and B can be determined via numerical optimization (see the Appendix E for details). (iii) To minimize the cross-coupling and leakage errors, one can also combine UDPs with the hyper-Gaussian function $g(t) = e^{-[2(t/T-1/2)]^8}$ of the optimal STIRAP pulses [43], i.e., $G(t) = \Omega_0 g(t)[1 + Ae^{-(t/T-1/2)^2/B^2}]$.

III. EXPERIMENTAL RESULTS AND ANALYSIS

In the following, we discuss an exemplary implementation of UDPs using superconducting quantum circuits [see Fig. 1(c)]. Specifically, we realize a state transfer process from $|0\rangle$ to $|2\rangle$ in an Xmon type of superconducting qutrit. To the first order of approximation, this specific system can be viewed as an anharmonic oscillator, with an anharmonicity about one order of magnitude smaller than its characteristic frequency. Such a small anharmonicity renders the Hamiltonian $H_0(t)$ introduced above insufficient to describe an Xmon qutrit driven by two microwave pulses. Additional terms describing cross-coupling and leakage to higher excited energy levels must be added to $H_0(t)$:

$$\begin{aligned}H(t) &= H_0(t) + \frac{1}{2} \\ &\times \left[\left(\frac{\Omega_S}{\sqrt{2}} e^{-i\alpha t} |0\rangle\langle 1| + \sqrt{2} \Omega_P e^{-i\alpha t} |1\rangle\langle 2| \right) + \text{H.c.} \right] \\ &+ \frac{1}{2} \left[\left(\frac{\sqrt{6} \Omega_S}{2} e^{-i\alpha t} + \sqrt{3} \Omega_P e^{-i2\alpha t} \right) |2\rangle\langle 3| + \text{H.c.} \right].\end{aligned}\quad (4)$$

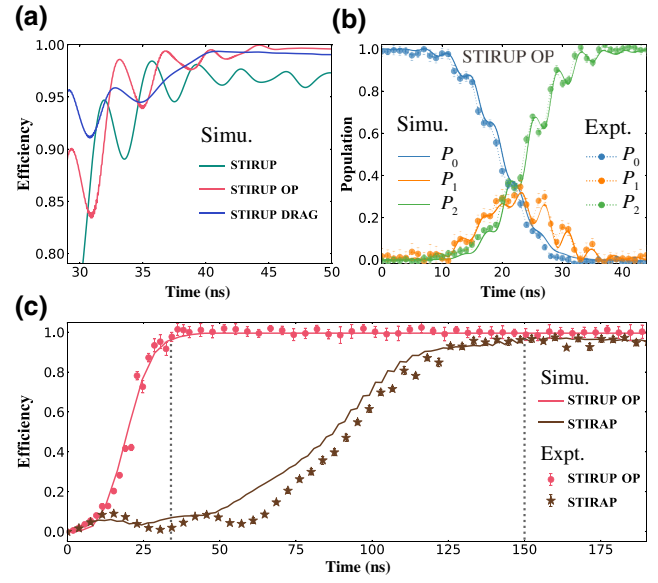


FIG. 2. Performance of UDPs. (a) Numerical simulation of the transfer efficiency (defined as the population of $|2\rangle$) towards the end of three different passages. The oscillatory behavior is due to the cross-coupling and leakage discussed in the main text. (b) Evolution of populations during a state transfer using the UDP OP passage. (c) Transfer efficiencies of two passages: STIRAP and UDP OP. The two dotted lines at 34 and 150 ns mark the moments when an efficiency of 96% is achieved for the UDP OP and STIRAP passages, respectively.

Here we consider only the leakage to state $|3\rangle$, and α is the anharmonicity of the Xmon defined as the difference between the lowest two frequencies of transition: $\alpha = f_{12} - f_{01}$. With such additional contribution, the pulses designed based on Eq. (3) [obtained for $H_0(t)$] no longer give proper passages for the desired transfer. Indeed, numerical simulations indicate that the transfer process using such pulses exhibits a strong oscillatory behavior towards the end, which leads to ambiguity in evaluating the transfer efficiency [see the UDP curve in Fig. 2(a)]. Such oscillatory behavior is due to the cross-coupling and leakage discussed above. In the following we demonstrate that by modifying the pulses designed based on Eq. (3) using certain optimizations, one can effectively suppress these unwanted effects and achieve the desired state transfer with high efficiency and fidelity.

Two different ways of optimization are investigated. In the first one, we adapt the method used in Refs. [43,44] for optimizing the STIRAP process. In the second one, we extend the standard method of derivative removal by adiabatic gate (DRAG) for a three-level system to include even higher excited states [45–48]. In both optimizations, we run numerical simulations, using a master equation, to optimize the overall fidelity of the transfer process. Both optimized and unoptimized pulses (hereafter referred to as UDP OP, UDP DRAG, and UDP, respectively), together

with those used in the STIRAP process, are compared in Fig. 1(d). Further details of pulse design and optimization can be found in Appendix E. With such optimizations, the oscillatory behavior mentioned above can be suppressed to a large extent. The transfer efficiency can now be determined to be 99.8% and 99.5% for the two optimizations, respectively [Fig. 2(a)].

All data reported in this work are acquired on one Xmon qutrit, and similar results are reproduced on other samples. The characteristic frequencies of the qutrit used here are around $f_{10} = \omega_{10}/2\pi = 5.208$ GHz and $f_{21} = \omega_{21}/2\pi = 4.958$ GHz. The relaxation and dephasing times are $T_1^{10} = 4.82$ μ s, $T_2^{10} = 5.06$ μ s, $T_1^{21} = 5.96$ μ s, and $T_2^{21} = 2.55$ μ s, respectively. External microwave drives are applied to the qutrit through an *XY* control line [49] (also see Fig. 13 in Appendix I). The qutrit is capacitively coupled to a resonator of quarter-wavelength ($\omega_r/2\pi = 6.68$ GHz), which is in turn coupled to a transmission line. The state of the qutrit can be deduced by measuring the transmission coefficient S_{21} of the transmission line using the dispersive readout scheme [49]. Further details of the sample and measurement setup can be found in Appendix I.

To characterize a state transfer process following a specific passage, we measure population of the three levels of the qutrit as a function of time. Figure 2(b) shows a typical data set for the case of the UDP OP passage. The qutrit is initialized to state $|0\rangle$, and the pulse shown on the third panel of Fig. 1(d) is applied. Within 44 ns, the population of state $|2\rangle$ rises to above 99%, accomplishing a fast and high-fidelity transfer from state $|0\rangle$ to $|2\rangle$. Figure 2(c) compares the efficiency of transfer (i.e., population of $|2\rangle$) for two different passages. For the STIRAP case, the maximum transfer efficiency (about 96%) is achieved at around 150 ns, whereas the UDP OP passage can reach the same efficiency within 34 ns. Such acceleration helps minimize losses due to spontaneous emission from excited states. As a result, the UDP can still achieve high fidelity even though the population of the intermediate state is nonzero during the transfer, whereas in STIRAP there is a negligible occupation of the intermediate state during the whole process. We also emphasize that while the UDPs used here do not specifically target at accelerating the transfer, like those STA-based variants of STIRAP, they nevertheless accomplish this goal nicely.

Next, we investigate the robustness of different protocols against experimental errors. In Fig. 3, the transfer efficiencies of five passages against the error in the Rabi frequency $\eta_{p,s}$ are compared to each other. $\eta_{p,s}$ is defined as $\tilde{\Omega}_{p,S} = (1 + \eta_{p,s})\Omega_{p,S}$, where $\tilde{\Omega}_{p,S}$ and $\Omega_{p,S}$ are actual and expected values of the Rabi frequency, respectively. For the resonant Rabi (RR) method [50,51], two identical π pulses in the form of $\Omega_{p,S} = \Omega_0 \sin \beta(t)$ are applied. The RR scheme is often used to benchmark protocols of state transfer and certain quantum gates. The STIRAP CD is an accelerated STIRAP protocol based on the counterdiabatic

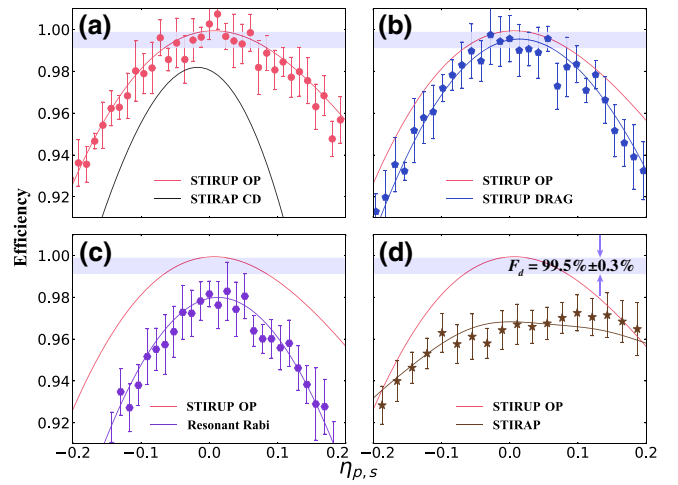


FIG. 3. Robustness of the transfer efficiency against error in the Rabi frequency for five different passages. In all four panels, lines are results of numerical simulations, symbols are experimental results, and the shaded stripes indicate a range of the efficiency of $(99.5 \pm 0.3)\%$. For comparison, the results of UDP OP passage are shown in all four panels. In (a), the black line (STIRAP CD) represents numerical simulation of a state transfer using STIRAP accelerated by a counterdiabatic (CD) driving, as reported in Ref. [30].

driving process [30] (see Appendix H for a detailed implementation). The UDP OP process has the best robustness in transfer efficiency against the error, larger than 92% in the range of $0.8\text{--}1.2\Omega_{p,S}$. Overall, the UDP OP passage is superior to the RR scheme, the STIRAP cases (both original and accelerated forms), and the UDP DRAG passage, in terms of both robustness and optimal transfer efficiency.

We also investigate, both numerically and experimentally, the effect of detuning in the pulse frequencies on the transfer efficiency of different methods. Figure 4 plots the transfer efficiency as a function of the two detunings defined by $\delta_1 = \omega_{d1} - \omega_{10}$ and $\delta_2 = \omega_{d2} - \omega_{21}$ [ω_{d1} and ω_{d2} are frequencies of the two external drives, see Fig. 1(a)]. The two methods using our optimization show similar performance. In both cases, the transfer efficiency is quite robust against the two detunings as long as their sum is kept near zero (i.e., the two-photon resonant condition is approximately held). Contours of the transfer efficiency can be easily identified in the set of experimental data, and are in reasonable agreement with the numerical simulations (see Appendix F for a comparison). Overall, the RR and the adiabatic passage cases exhibit less robust performance against the detuning errors. Moreover, we also run numerical simulations to compare our protocols to the scheme of STIRAP accelerated by a counterdiabatic driving [30], and find a better robustness in the transfer efficiency against experimental errors for our protocols.

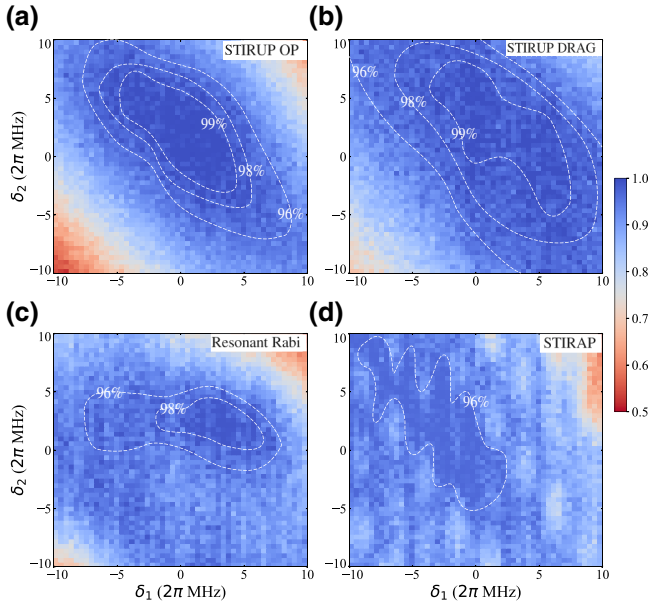


FIG. 4. Robustness of the transfer efficiency against detuning errors $\delta_{1,2}$ for four different passages: (a) UDP OP, (b) UDP DRAG, (c) resonant Rabi, and (d) STIRAP. Dashed lines are contours indicating different values of the efficiency. All four panels are experimental results, and their comparison to numerical simulations can be found in Fig. 11 in Appendix F.

The Xmon superconducting qutrit used here for demonstration has a Ξ configuration. For completeness, we also perform numerical simulations for another popular case, the Λ configuration (see Appendix B and C for details). Overall speaking, UDPs offer a handy flexibility of customization for different tasks of coherent quantum control. When speed is not the first priority, UDPs can be pushed to the adiabatic limit and automatically reduces to STIRAP. In many other cases, it is possible to find a balance between efficiency and performance. One particular interesting result is that UDPs can still deliver decent results even in cases of non-negligible to moderate dephasing, a welcome feature for quantum-information processing. Furthermore, UDPs can be generalized to more sophisticated applications. For example, some of the authors of this work have shown theoretically that UDPs can be used for state transfer and one-step generation of entanglement in multiqubit systems [40].

IV. CONCLUSION

In summary, we propose and demonstrate UDPs as a simple and flexible protocol for quantum control. In this protocol, user-defined passages for realizing any specified quantum control are constructed via direct engineering of parameterized solutions of the Schrödinger equation. The essential idea of UDPs does not depend on assumptions

specific to particular systems, so it should be readily implementable on other platforms. In the current work, UDPs need to be optimized to eliminate the cross-coupling and leakage errors prevailing in Xmon types of superconducting devices, due to their relatively small anharmonicity. It therefore should be expected that on other platforms with larger anharmonicity, the application of UDPs could be even more straightforward. Meanwhile, there always exists the flexibility of incorporating optimizations designed for specific systems. Finally, we note that the idea of using parameterized states for solving Schrödinger's equation can be extended to nonlinear systems; for some cases, the population of the intermediate state must be nonzero [38].

ACKNOWLEDGMENTS

This work is supported by the Key-Area Research and Development Program of Guang-Dong Province (Grant No. 2018B030326001), the National Natural Science Foundation of China (Grant No. U1801661,12074166), the Guangdong Innovative and Entrepreneurial Research Team Program (Grant No. 2016ZT06D348), the Guangdong Provincial Key Laboratory (Grant No. 2019B121203002), the Science, Technology and Innovation Commission of Shenzhen Municipality (Grant No. KYT-DPT20181011104202253), the Shenzhen Science and Technology Basic Research Program (Grant No. JCYJ20170817105201098), the Shenzhen-Hong Kong Cooperation Zone for Technology and Innovation (Grant No. HZQB-KCZYB-2020050), and the NSF of Beijing (Z190012).

APPENDIX A: GENERAL FRAME OF UDP

Let us consider a three-level system driven by two resonant external fields:

$$H_0(t) = \frac{1}{2} \begin{bmatrix} 0 & \Omega_P(t) & 0 \\ \Omega_P^*(t) & 0 & \Omega_S(t) \\ 0 & \Omega_S^*(t) & 0 \end{bmatrix}. \quad (\text{A1})$$

A general solution of the corresponding Schrödinger equation can be written into the following form:

$$|\Phi_{\text{UD}}(t)\rangle = [a_0(t), a_1(t), a_2(t)]^T, \quad (\text{A2})$$

where the time-dependent coefficients $a_n(t)$ satisfy the normalized condition, i.e., $\sum_{n=0}^2 |a_n(t)|^2 = 1$. Plugging this solution into the Schrödinger equation, one obtains

$$\begin{aligned} \Omega_P(t) &= \frac{2i\partial_t a_0}{a_1}, & \Omega_S^*(t) &= \frac{2i\partial_t a_2}{a_1}, \\ a_0\partial_t a_0^* + a_1^*\partial_t a_1 + a_2\partial_t a_2^* &= 0. \end{aligned} \quad (\text{A3})$$

In UDP, a convenient parameterization of the general solution that satisfies the above equation is used:

$$(a_0, a_1, a_2)^T = (\cos\gamma \cos\beta, e^{i\phi_1} \sin\gamma, -e^{i\phi_2} \cos\gamma \sin\beta)^T, \quad (\text{A4})$$

with such parameterization, customized passages can be designed by engineering the time-dependent parameters $\gamma(t)$ and $\beta(t)$, and the two phase constants $\phi_{1,2}$. To eliminate the effects of phase factors, we can choose $\phi_1 = \pi/2$ and $\phi_2 = 0$ for simplicity. In particular, in the following we show that both the original STIRAP and its various accelerated versions can be produced as different customized passages in the frame of UDP.

APPENDIX B: GENERATION OF STIRAP BY UDP

Let us first review the STIRAP process. The Hamiltonian given in Eq. (A1) has three instantaneous eigenstates:

$$\begin{aligned} |E_{\pm}(t)\rangle &= \frac{1}{\sqrt{2}} [\sin\theta(t)|0\rangle \pm |1\rangle + \cos\theta(t)|2\rangle], \\ |D_0(t)\rangle &= \cos\theta(t)|0\rangle - \sin\theta(t)|2\rangle, \end{aligned} \quad (\text{B1})$$

with corresponding eigenenergies $E_{\pm}(t) = \pm\Omega_{\text{rms}}(t)/2$ and $D_0 = 0$, respectively. Here $\Omega_{\text{rms}}(t) = \sqrt{\Omega_P^2(t) + \Omega_S^2(t)}$ and the mixing angle $\theta(t) = \arctan[\Omega_P(t)/\Omega_S(t)]$. The state $|D_0(t)\rangle$ is a dark state since it is dynamically decoupled from the system evolution. STIRAP uses this dark state to accomplish a coherent population transfer from $|0\rangle$ to $|2\rangle$, without incurring a significant occupation of the state $|1\rangle$, thus avoiding the loss due to spontaneous emission of the intermediate state. In order to keep the system evolving in the dark state, the local adiabatic condition must be satisfied [1,41]:

$$\Omega_{\text{rms}}(t) \gg |\dot{\theta}(t)| = \frac{|\Omega_S(t)\dot{\Omega}_P(t) - \Omega_P(t)\dot{\Omega}_S(t)|}{\Omega_P^2(t) + \Omega_S^2(t)}. \quad (\text{B2})$$

When the above adiabatic condition is satisfied, the dark state $|D_0(t)\rangle$ is an approximate solution of the Schrödinger equation, i.e.,

$$i\hbar \frac{\partial}{\partial t} |D_0(t)\rangle \approx H_0(t) |D_0(t)\rangle. \quad (\text{B3})$$

Therefore, the STIRAP scheme can be viewed as one customized UDP $|\Phi_{\text{UD}}(t)\rangle = \cos\gamma \cos\beta(t)|0\rangle + i \sin\gamma |1\rangle - \cos\gamma \sin\beta(t)|2\rangle$, with the control parameters $\theta(t) = \beta(t)$ and $\gamma(t) \approx 0$ in the adiabatic limit. To further illustrate this point, we numerically study the asymptotic behavior of the UDPs. The results are shown in Fig. 5, where three relevant quantities are plotted as functions of the evolution time T . As T increases, the maximum population of the intermediate state continues to decrease, approaching the

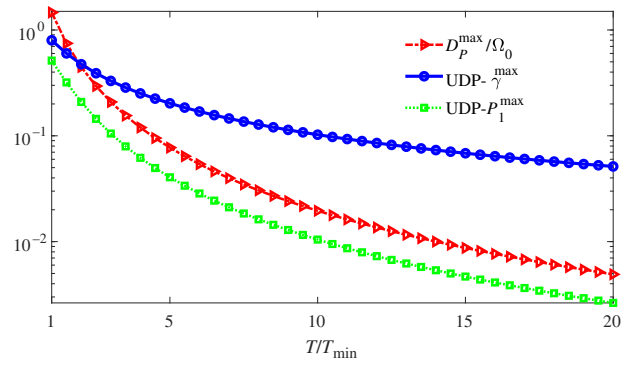


FIG. 5. Asymptotic behavior of UDP characterized by three relevant parameters: the maximum difference between the amplitudes of the UPD and STIRAP pulses (as defined in the text; here normalized to the characteristic pulse amplitude Ω_0), the maximum population of the intermediate state $|1\rangle$, and the maximum value of the control parameter $\gamma(t)$. Here the evolution time T is normalized to a minimum evolution time T_{min} of the UDP. With this minimum time, the UDP pulse during the whole evolution is no stronger than the maximum value of the STIRAP pulse. The longer the T is, the weaker the UDP pulse becomes. For the numerical simulation presented here, $T_{\text{min}} = 30.4$ ns. Other control parameters of the pulses are given in Table I.

STIRAP scheme. In addition, we also define a pulse distance $D_P(t) = |\Omega_P^{\text{UDP}}(t) - \Omega_P^{\text{STIRAP}}(t)|$ to evaluate the gap between STIRAP and UDP. Figure 5 shows that the maximum value of such difference also approaches zero in the adiabatic limit.

APPENDIX C: UDPs IN REALISTIC SYSTEMS WITH DECOHERENCE

STIRAP is robust against the population decay from the intermediate state, but this benefit is achieved at the cost of much elongated evolution time in order to satisfy the adiabatic condition. Such long evolution time not only reduces efficiency, but also makes STIRAP sensitive to dephasing errors [41]. UDPs, on the other hand, can be easily tailored to adapt the different characteristics of various quantum systems. In particular, as we show in the following, our numerical simulation indicates that UDPs can still deliver rather good performance in dephasing-limited systems.

Our numerical simulation is based on a master equation approach. When taking into account decoherence, the density matrix $\rho(t)$ of a quantum system satisfies the Lindblad master equation:

$$\begin{aligned} \frac{d}{dt} \rho(t) &= -\frac{i}{\hbar} [H(t), \rho(t)] + \sum_j \\ &\times \left[2L_j \rho(t) L_j^\dagger - \{L_j^\dagger L_j, \rho(t)\} \right]. \end{aligned} \quad (\text{C1})$$

TABLE I. Pulse information used in our experiments.

Passage	Experimental parameters		
	Pulse shape	Rabi frequency	Characteristic time
UDP	$\Omega_p = \sqrt{\Omega_0^2 f^2(t) + \dot{\gamma}^2(t)} \sin[\beta(t) + \eta(t)]$ $\Omega_s = \sqrt{\Omega_0^2 f^2(t) + \dot{\gamma}^2(t)} \cos[\beta(t) + \eta(t)]$	$\Omega_0 = 0.04 (2\pi)$ GHz	$T = 44$ ns
UDP OP	$\tilde{\Omega}_p = \sqrt{\Omega_0^2 g^2(t) f^2(t) + \dot{\gamma}^2(t)} \sin[\beta(t) + \eta(t)]$ $\tilde{\Omega}_s = \sqrt{\Omega_0^2 g^2(t) f^2(t) + \dot{\gamma}^2(t)} \cos[\beta(t) + \eta(t)]$ $g(t) = e^{-(2t)^8}$	$\Omega_0 = 0.04 (2\pi)$ GHz	$T = 44$ ns
UDP DRAG	$\Omega_p = \sqrt{\Omega_0^2 f^2(t) + \dot{\gamma}^2(t)} \sin[\beta(t) + \eta(t)]$ $\Omega_s = \sqrt{\Omega_0^2 f^2(t) + \dot{\gamma}^2(t)} \cos[\beta(t) + \eta(t)]$ $\tilde{\Omega}_p(t) = \Omega_p - i(A/\alpha)d\Omega_p/dt, \tilde{\Omega}_s(t) = \Omega_s - i(B/\alpha)d\Omega_s/dt$	$\Omega_0 = 0.039(2\pi)$ GHz	$T = 44$ ns
STIRAP	$\Omega_p = \Omega_0 \sin \beta(t)$ $\Omega_s = \Omega_0 \cos \beta(t)$	$\Omega_0 = 0.04(2\pi)$ GHz	$T = 196$ ns
Resonant Rabi	$\Omega_{p,s} = \Omega_0 \sin \beta(t)$	$\Omega_0 = 0.04 (2\pi)$ GHz	$T = 36$ ns

Here $H(t)$ is the Hamiltonian of the quantum system. $L_j = \sqrt{\gamma_j} A_j$ are terms that characterize decoherence, including both relaxation and dephasing, with A_j and γ_j being the relevant operators and the corresponding rates, respectively (see the following discussion for exact forms of L_j in different systems).

In the following, using numerical simulations based on the above approach, we compare UDP and STIRAP for realizing a coherent population transfer in a general three-level system subjected to decoherence, in both Λ and Ξ configurations.

1. Λ -system

For this case, the Hamiltonian is $H_0(t)$ in Eq. (A1) and the decoherence is described by the following terms:

$$L_j = \sqrt{\Gamma_1^{10}}|0\rangle\langle 1|, \sqrt{\Gamma_1^{12}}|2\rangle\langle 1|, \sqrt{\Gamma_2^{10}}(|1\rangle\langle 1| - |0\rangle\langle 0|), \\ \times \sqrt{\Gamma_2^{12}}(|1\rangle\langle 1| - |2\rangle\langle 2|). \quad (C2)$$

The simulation results are shown in Fig. 6. Here we simulate two different cases: with and without external relaxation. For simplicity, we set all relaxation rates to be identical, and all dephasing rates to be identical. The UDP method using slow pulses (approaching the adiabatic limit) has similar performance as STIRAP, as expected. The presence of external relaxation does not affect STIRAP and UDP-slow cases by much, which is also expected since during the transfer, the population of state $|1\rangle$ is negligible. In both STIRAP and UDP-slow cases, the efficiency is much more sensitive to dephasing than to relaxation. On the other hand, the UDP method using fast pulses is more sensitive to relaxation. It performs better than STIRAP and UDP slow in the dephasing-limited range (area close to the vertical axis).

The results presented in Fig. 6 demonstrate that there is much flexibility in designing the UDP pulses. If efficiency is not the first priority, one can design the UDP pulse in the adiabatic limit and always achieve nearly identical performance as STIRAP. On the other hand, for many dephasing-limited systems used for quantum-information processing, the UDP scheme can still be customized to deliver high efficiency.

2. Ξ system

For this case, the Hamiltonian is $H_0(t)$ in Eq. (A1) and the decoherence is described by the following terms:

$$L_j = \sqrt{\Gamma_1^{10}}|0\rangle\langle 1|, \sqrt{\Gamma_1^{21}}|1\rangle\langle 2|, \sqrt{\Gamma_2^{10}}(|1\rangle\langle 1| - |0\rangle\langle 0|), \\ \times \sqrt{\Gamma_2^{21}}(|2\rangle\langle 2| - |1\rangle\langle 1|). \quad (C3)$$

The simulation results are shown in Figs. 7 and 8. Here we do not include external relaxation since it is negligible in most realistic Ξ systems. Figure 7 is for a general Ξ system without significant cross-coupling ($f_{01} = 5$ GHz, $f_{12} = 2.5$ GHz). Both STIRAP and UDP-slow pulses deliver rather poor results even with moderate internal relaxation. This is not surprising since these two methods are designed for minimizing the population of the intermediate state, but in a Ξ system the loss due to the relaxation from the highest lying final state also degrades the transfer efficiency. In such a case, an accelerated state transfer, like that achieved via UDP-fast pulses, is very welcome. Figure 8 shows the simulation results for a Ξ system with a significant cross-coupling ($f_{01} = 5$ GHz, $f_{12} = 4.75$ GHz), like the superconducting Xmon qubit used in this work. In this case, all three methods perform worse than the case with negligible cross-coupling.

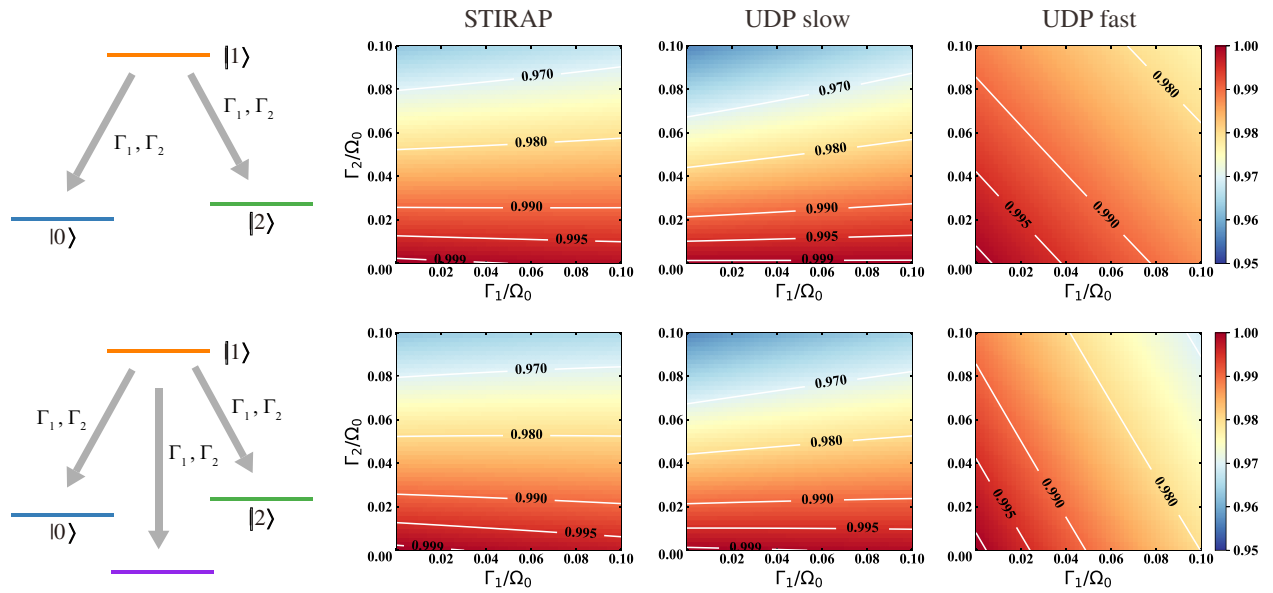


FIG. 6. Efficiency of a population transfer in a general three-level Λ system subjected to decoherence, using STIRAP, UDP-slow, and UDP-fast pulses. Upper panel corresponds to the case with only internal relaxation, and the lower panel takes into account external relaxation as well. For simplicity, we set all relaxation rates to Γ_1 and all dephasing rates to Γ_2 , and normalize all rates to the characteristic pulse amplitude Ω_0 (see Table I for pulse information). The evolution times are $10\Omega_0^{-1}$ for STIRAP and UDP-slow pulses, and $1.76\Omega_0^{-1}$ for the UDP-fast case.

APPENDIX D: PRODUCING THE ACCELERATED VARIANTS OF STIRAP BY UDP

Various techniques under the name “shortcuts to adiabaticity” and inverse engineering have been proposed to speed up adiabatic processes, including the STIRAP scheme. For example, Baksic *et al.* [33] proposed a dressed-state method that can change the dynamics of the original Hamiltonian by adding additional terms. In this method, an alternative basis of dressed states are defined as

$$|\tilde{E}_{\pm}\rangle = \sin\theta(\cos\xi \mp i\sin\xi\cos\mu) \pm i\cos\theta\sin\mu|0\rangle \\ \pm \cos\xi\cos\mu - i\sin\xi|1\rangle + \cos\theta(\cos\xi$$

$$\mp i\sin\xi\cos\mu) \mp i\sin\theta\sin\mu|2\rangle,$$

$$|\tilde{E}_0\rangle = \sin\theta\sin\mu\sin\xi + \cos\theta\cos\mu|0\rangle + i\sin\mu\cos\xi|1\rangle \\ + \cos\theta\sin\mu\sin\xi - \sin\theta\cos\mu|2\rangle. \quad (\text{D1})$$

The state $|\tilde{D}_0\rangle$ is used for state transfer. This scheme can also be produced in the frame of UDP by setting

$$a_0 = \sin\theta\sin\mu\sin\xi, a_1 = i\sin\mu\cos\xi, \\ a_2 = \cos\theta\sin\mu\sin\xi - \sin\theta\cos\mu. \quad (\text{D2})$$

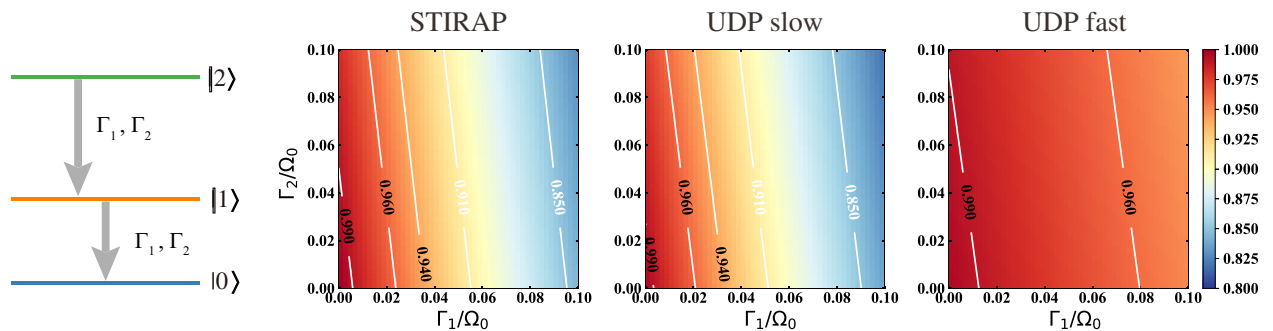


FIG. 7. Efficiency of a population transfer in a general three-level Ξ system subjected to decoherence, using STIRAP, UDP-slow, and UDP-fast pulses. Here $f_{01} = 5$ GHz, $f_{12} = 7.5$ GHz. For simplicity, we set all relaxation rates to Γ_1 and all dephasing rates to Γ_2 , and normalize all rates to the characteristic pulse amplitude Ω_0 . The evolution times are $10\Omega_0^{-1}$ for STIRAP and UDP-slow pulses, and $1.76\Omega_0^{-1}$ for the UDP-fast case.

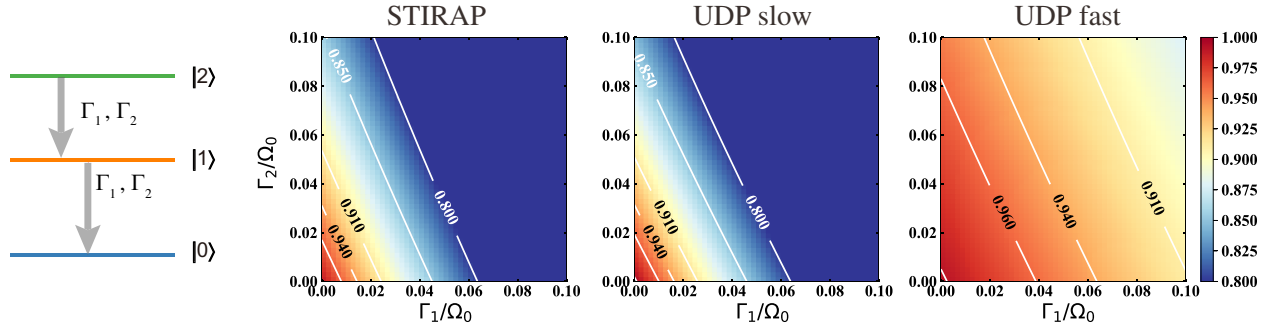


FIG. 8. Efficiency of a population transfer in a three-level Ξ system with significant cross-coupling subjected to decoherence, using STIRAP, UDP-slow, and UDP-fast pulses. Here $f_{01} = 5$ GHz, $f_{12} = 4.75$ GHz. This is similar to the conditions for the experiment reported in the main paper. For simplicity, we set all relaxation rates to Γ_1 and all dephasing rates to Γ_2 , and normalize all rates to the characteristic pulse amplitude Ω_0 . The evolution times are $10\Omega_0^{-1}$ for STIRAP and UDP-slow pulses, and $1.76\Omega_0^{-1}$ for the UDP-fast case. The relative anharmonicity, as defined by $(\omega_{21} - \omega_{10})/\omega_{10}$, is -0.05 .

Combining Eqs. (D2) and (A3), one has the following pulse shape:

$$\begin{aligned}\Omega_P(t) &= \sqrt{W_0^2(t) + W_1^2(t)} \sin \left[\theta(t) - \arctan \left(\frac{W_0(t)}{W_1(t)} \right) \right], \\ \Omega_S(t) &= \sqrt{W_0^2(t) + W_1^2(t)} \cos \left[\theta(t) - \arctan \left(\frac{W_0(t)}{W_1(t)} \right) \right],\end{aligned}\quad (\text{D3})$$

where, $W_0(t) = \dot{\mu}/\cos \zeta - \dot{\theta} \tan \zeta$ and $W_1(t) = \dot{\zeta} + \dot{\mu} \sin \zeta - \dot{\theta}/\tan \mu \cos \zeta$. These results are identical to those obtained by Baksic *et al.* [33]. Therefore, the passage based on the dressed-state method can be viewed as a particular case of UDP.

Similarly, a link between the dynamical invariant approach in Ref. [34] and UDP can also be established by setting the UDP $|\Phi(t)\rangle$ to be the instantaneous eigenstate $|\phi_0(t)\rangle = \cos \gamma \cos \beta |0\rangle - i \sin \gamma |1\rangle - \cos \gamma \sin \beta |2\rangle$ of the dynamical invariant $I(t)$ with $\phi_1 = -\pi/2$. Note that the dynamical invariant is difficult to find because of the requirement of dynamical symmetry for the original Hamiltonian. On the other hand, the UDP approach relies on finding and engineering exact solutions of the Schrödinger equation, but not on specific dynamical symmetry of the Hamiltonian.

APPENDIX E: PULSE DESIGN FOR UDPS

The pulses can alternatively be determined by $G(t)$ and $\beta(t)$. We further set $G(t) = \Omega_0 g(t) f(t)$, and use Ω_0 for controlling pulse amplitude, $g(t)$ for optimization to suppress the cross-coupling and leakage errors, and $f(t)$ for reducing the population of the intermediate state, respectively. Let us first consider UDP without optimization, namely, $g(t) = 1$, $f(t)$ and $\beta(t)$ are chosen as $f(t) = 1 + Ae^{-(t/T-1/2)^2/B^2}$ and $\beta(t) = \pi/2/1 + e^{-m_c(t/T-1/2)}$ with T

being the pulse length and m_c being a constant for controlling the boundary condition for state transfer. For example, for a transfer from state $|0\rangle$ to $|2\rangle$, we set $m_c = 10$ so that β approaches 0 and $\pi/2$ for $t \rightarrow 0$ and $t \rightarrow \pi/2$, respectively. The final form of the pulses is given in Table I.

Next, to minimize the cross-coupling and leakage errors, we apply the well-known Dykhne-Davis-Pechukas (DDP) [43,44] or DRAG [45–47] methods to optimize the above UDP, named “UDP OP” and “UDP DRAG,” respectively.

For UDP OP, we use the hyper-Gaussian function $g(\tau) = e^{-[2(t/T-1/2)]^8}$ as a mask [see Table I as well as Fig. 1(d) in the main text]. There are three tunable parameters, A , B , and pulse length T , that need to be determined. Since a major objective is to accelerate the state transfer process, T should not be too long. On the other hand, the effect of cross-coupling will become significant if the operation time is too short. Therefore, we set a range of 30–80 ns for T , and optimize A and B at different selected values of T by numerical

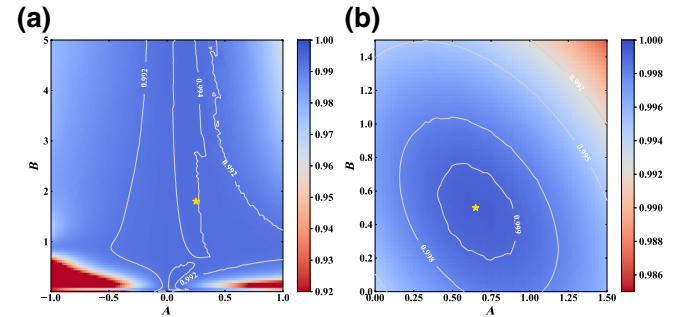


FIG. 9. Parameter optimization for the (a) UDP OP and (b) UDP DRAG protocols, respectively. The transfer efficiency is numerically simulated as a function of A and B . The star symbols indicate the points where the highest efficiency is achieved. For both panels, $T = 44$ ns.

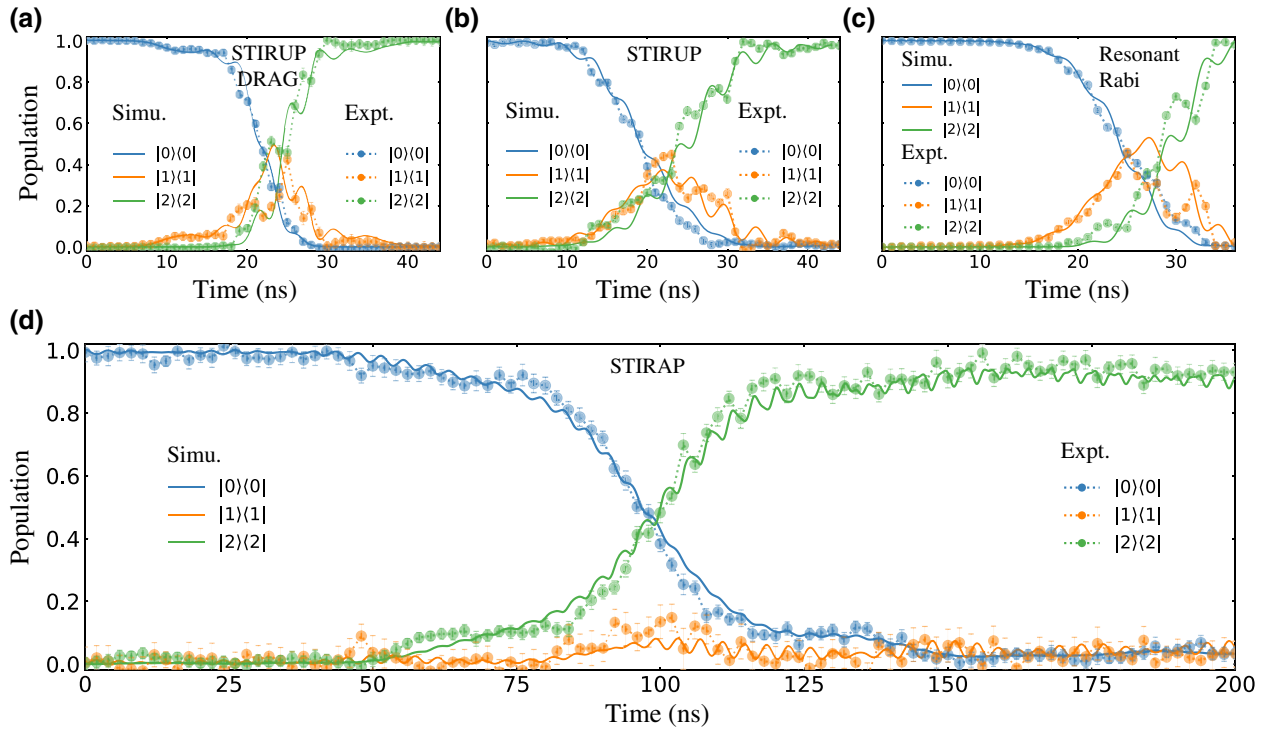


FIG. 10. Evolution of populations during state transfer for four different passages. The solid and dashed lines (with symbols) show numerical simulations and experimental results, respectively.

simulations using a master-equation method. Moreover, amplitude of the pulses must be kept at a reasonable level (not too high for realistic electronics), which also sets limits for A and B . With all the above considerations, the

parameters are searched and determined using a gradient-descent method. Figure 9 shows the result of numerical simulation at $T = 44$ ns for the UDP OP protocol, from which the optimal parameters are determined to be

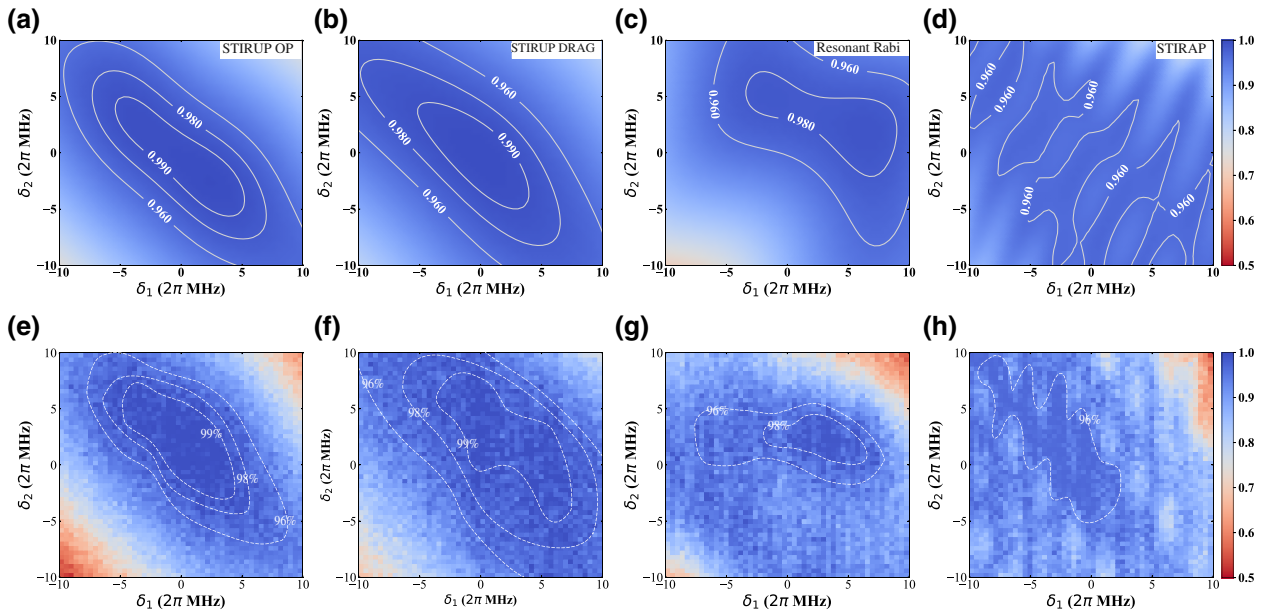


FIG. 11. Robustness of transfer efficiency against detuning errors (defined in the main text) for four different passages. (a)–(d) and (e)–(h) show numerical simulations and experimental results, respectively.

TABLE II. Comparison with other related experimental works.

Passage	Transfer efficiency	Evolution time (ns)	Relaxation times (μs)	Dephasing times (μs)	Anharmonicity (MHz)
UDP OP (this work)	99.5%	44	$T_1^{10} \approx 4.8$ $T_1^{21} \approx 6$	$T_2^{10} \approx 5$ $T_2^{21} \approx 2.5$	250
STIRAP CD [30]	96%	140	$T_1^{10} \approx 1.7$ $T_1^{21} \approx 1.2$	$T_2^{10} \approx 11$ $T_2^{21} \approx 11$	370
STIRAP [4]	97%	600	$T_1^{10} \approx 12$ $T_1^{21} \approx 7.6$	$T_2^{10} \approx 5$ $T_2^{21} \approx 5$	225
STIRAP [3]	83%	92	$T_1^{10} \approx 0.4$ $T_1^{21} \approx 0.2$	$T_2^{10} \approx 2.5$ $T_2^{21} \approx 2.5$	450

$A = 0.25$, $B = 1.8$, corresponding to a transfer efficiency of 99.94%.

For UDP DRAG, we apply the DRAG correction by setting $\beta(t) = \arctan \left[\frac{2(t - \tau_1)\tau_2/(t - T/2)^2}{e^{-(t - \tau_1)^2 + \tau_2^2/2/(T/8)^2}} \sqrt{2 \cosh \left[(t - \tau_1) \tau_2 / (T/8)^2 \right]} \right]$, $\Omega(t) = \Omega_0$, and $f(t) = \{1 + 1/5\Omega(t)T \cosh[\eta(t - \tau_1)]\}$, with $\tau_1 = 7T/20$, $\tau_2 = 3T/20$, and $\eta = 9/80T$. Here, we extend the DRAG method to a three-level system by adding time derivative $\tilde{\Omega}_{P,S}$ to the quadrature components:

$$\tilde{\Omega}_P(t) = \Omega_P - i \frac{A}{\alpha} \frac{d\Omega_P}{dt}, \quad \tilde{\Omega}_S(t) = \Omega_S - i \frac{B}{\alpha} \frac{d\Omega_S}{dt}, \quad (\text{E1})$$

where A and B are weighting parameters, and α is the anharmonicity of our Xmon qubit (approximately 250 MHz). Figure 9 shows the result of numerical simulation for the case of $\Omega_0 = 2\pi \times 39$ MHz and $T = 44$ ns. The highest transfer efficiency of 99.93% is achieved at $A = 0.65$ and $B = 0.5$. The corresponding pulse envelopes are shown in Fig. 1(d) in the main text.

APPENDIX F: EVOLUTION OF POPULATION DURING TRANSFER FOR OTHER PASSAGES

Figure 10 shows evolution of populations during state transfer for four different passages. This figure is to be compared to Fig. 2(b) in the main text where similar data is shown for the UDP OP passage.

Figure 11 compares robustness of transfer efficiency against detuning errors, including both numerical simulations and experimental results, for four different passages. The two passages based on UDP show better agreement between simulations and experimental data. Overall, they also deliver a better performance compared to the other two passages.

APPENDIX G: COMPARISON WITH OTHER EXPERIMENTS PERFORMED IN SUPERCONDUCTING QUANTUM CIRCUITS

Table II compares our results to some other representative experiments on state transfer performed in superconducting quantum circuits. Overall, the UDP OP approach delivers the best performance.

APPENDIX H: COMPARISON WITH STIRAP CD PROCESS

Recently, Vepsalainen *et al.* [30] implemented a superadiabatic state transfer protocol based on the counterdiabatic driving (CD) method in a superconducting qutrit. The CD Hamiltonian for acceleration is realized via a third microwave pulse, in addition to the two STIRAP pulses, that corresponds to a two-photon process. We adapt the essence of this approach and created an accelerated passage of state transfer termed ‘‘STIRAP CD.’’ In the following, we compare STIRAP CD to UDP OP using numerical simulations.

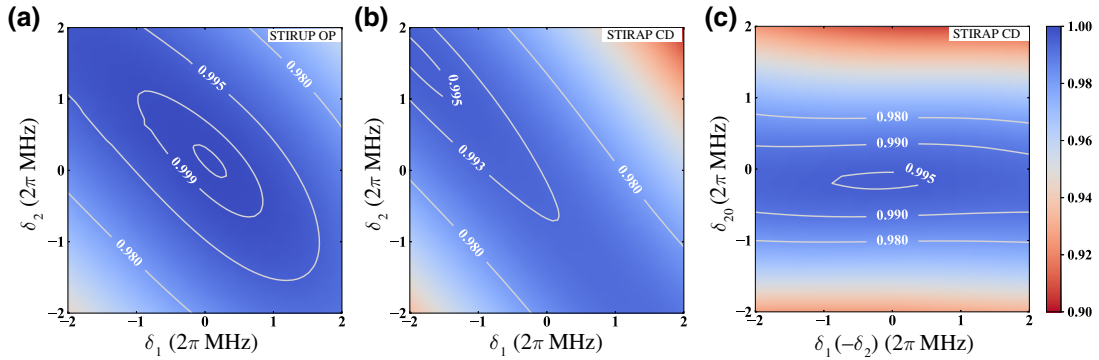


FIG. 12. Numerical simulation of the robustness of transfer efficiency against detuning errors for (a) UDP OP and (b),(c) STIRAP CD passages. Here $\delta_1 = \omega_{d1} - \omega_{01}$, $\delta_2 = \omega_{d2} - \omega_{12}$, $\delta_{20} = \omega_{d20} - (\omega_{10} + \omega_{21})/2$. For STIRAP CD, an additional detuning error δ_{20} exists for the CD pulse. $\delta_{20} = 0$ in (b), and $\delta_1 + \delta_2 = 0$ in (c).

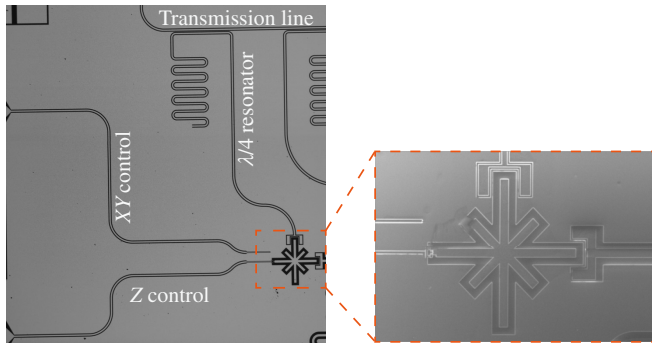


FIG. 13. Left: optical image of one sample used in this work. Right: SEM image of the Xmon qubit and its coupling capacitors.

For STIRAP CD, three microwave pulses are used:

$$\begin{aligned}\Omega_P(t) &= \Omega_0 \sin \beta(t), \\ \Omega_S(t) &= \Omega_0 \cos \beta(t), \\ \Omega_{CD}(t) &= \Omega_{P0} e^{-i(-\lambda_1/4 + \phi_i)}.\end{aligned}\quad (\text{H1})$$

The first two are the STIRAP pulses, and the third one is for realizing the counterdiabatic driving. The detuning, phase, and amplitude of the CD pulse are $\Delta_0 = \alpha/2$, $\phi_i = \pi/1.15$, and $\Omega_{P0} = 1.05 \sqrt{-2\sqrt{2}\Delta_0\theta} e^{-i(-\lambda_1/4 + \phi_i)}$, respectively. Here $\beta(t) = \pi/2/1 + e^{-m_c(t/T-1/2)}$, $\alpha/2\pi = 250$ MHz (anharmonicity), $\theta = \pi m_c e^{-m_c(t/T-1/2)} / 2T(e^{-m_c(t/T-1/2)} + 1)^2$, $\lambda_1 = (\sqrt{2}\pi) / [2e^{(-m_c/2)} + 1] - (\sqrt{2}\pi) / (2e^{(-m_c(t/T-1/2))} + 1)$ (T and m_c are defined previously in Sec. C). This pulse couples the two states $|0\rangle$ and $|2\rangle$ via a two-photon process, and corresponds to a CD Hamiltonian $H_{CD}(t) = \frac{1}{2} [\dot{\beta}(t) e^{-i(\pi/2)} |0\rangle\langle 2| + \text{H.c.}]$.

Figure 12 compares the robustness of transfer efficiency against detuning errors between the UDP OP and STIRAP CD methods. For a fair comparison, the pulse length T is set to be 88 ns where STIRAP CD achieves its best performance in our simulation, even though the UDP OP passage can accomplish the transfer process in 44 ns as reported in the main text. The UDP OP approach achieves a significantly better performance with only two microwave pulses.

APPENDIX I: SAMPLE INFORMATION

Figure 13 shows optical images of one of the samples. The qubit consists of a superconducting quantum interference device loop with two symmetric Josephson junctions. It is dispersively coupled to a $\lambda/4$ resonator for readout. The microwave pulses are introduced through the XY -control line, and a current is applied through the Z -control line to bias the qubit to the desired frequency [49,52,53].

[1] K. Bergmann, H. Theuer, and B. W. Shore, Coherent population transfer among quantum states of atoms and molecules, *Rev. Mod. Phys.* **70**, 1003 (1998).

[2] L. F. Wei, J. R. Johansson, L. X. Cen, S. Ashhab, and F. Nori, Controllable Coherent Population Transfers in Superconducting Qubits for Quantum Computing, *Phys. Rev. Lett.* **100**, 113601 (2008).

[3] K. S. Kumar, A. Vepsäläinen, S. Danilin, and G. S. Paraoanu, Stimulated Raman adiabatic passage in a three-level superconducting circuit, *Nat. Commun.* **7**, 10628 (2016).

[4] H. K. Xu, C. Song, W. Y. Liu, G. M. Xue, F. F. Su, H. Deng, Y. Tian, D. N. Zheng, S. Han, Y. P. Zhong, H. Wang, Y.-x. Liu, and S. P. Zhao, Coherent population transfer between uncoupled or weakly coupled states in ladder-type superconducting qutrits, *Nat. Commun.* **7**, 11018 (2016).

[5] R. G. Unanyan and M. Fleischhauer, Decoherence-Free Generation of Many-Particle Entanglement by Adiabatic Ground-State Transition, *Phys. Rev. Lett.* **90**, 133601 (2003).

[6] I. E. Linington and N. V. Vitanov, Decoherence-free preparation of Dicke states of trapped ions by collective stimulated Raman adiabatic passage, *Phys. Rev. A* **77**, 062327 (2008).

[7] S. P. Premaratne, F. C. Wellstood, and B. S. Palmer, Microwave photon Fock state generation by stimulated Raman adiabatic passage, *Nat. Commun.* **8**, 14148 (2017).

[8] J. A. Jones, V. Vedral, A. Ekert, and G. Castagnoli, Geometric quantum computation using nuclear magnetic resonance, *Nature* **403**, 869 (2000).

[9] L.-M. Duan, J. I. Cirac, and P. Zoller, Geometric manipulation of trapped ions for quantum computation, *Science* **292**, 1695 (2001).

[10] Z. Kis and F. Renzoni, Qubit rotation by stimulated Raman adiabatic passage, *Phys. Rev. A* **65**, 032318 (2002).

[11] R. G. Unanyan and M. Fleischhauer, Geometric phase gate without dynamical phases, *Phys. Rev. A* **69**, 050302 (2004).

[12] J. K. Pachos and A. Beige, Decoherence-free dynamical and geometrical entangling phase gates, *Phys. Rev. A* **69**, 033817 (2004).

[13] X. Lacour, N. Sangouard, S. Guérin, and H. R. Jauslin, Arbitrary state controlled-unitary gate by adiabatic passage, *Phys. Rev. A* **73**, 042321 (2006).

[14] D. Møller, J. L. Sørensen, J. B. Thomsen, and M. Drewsen, Efficient qubit detection using alkaline-earth-metal ions and a double stimulated Raman adiabatic process, *Phys. Rev. A* **76**, 062321 (2007).

[15] C. Menzel-Jones and M. Shapiro, Robust operation of a universal set of logic gates for quantum computation using adiabatic population transfer between molecular levels, *Phys. Rev. A* **75**, 052308 (2007).

[16] D. Møller, L. B. Madsen, and K. Mølmer, Quantum Gates and Multiparticle Entanglement by Rydberg Excitation Blockade and Adiabatic Passage, *Phys. Rev. Lett.* **100**, 170504 (2008).

[17] B. Rousseaux, S. Guérin, and N. V. Vitanov, Arbitrary qubit gates by adiabatic passage, *Phys. Rev. A* **87**, 032328 (2013).

[18] B. B. Zhou, P. C. Jerger, V. O. Shkolnikov, F. J. Heremans, G. Burkard, and D. D. Awschalom, Holonomic Quantum Control by Coherent Optical Excitation in Diamond, *Phys. Rev. Lett.* **119**, 140503 (2017).

[19] U. Gaubatz, P. Rudecki, S. Schiemann, and K. Bergmann, population transfer between molecular vibrational levels

- by stimulated Raman scattering with partially overlapping laser fields. A new concept and experimental results, *J. Chem. Phys.* **92**, 5363 (1990).
- [20] J. R. Kuklinski, U. Gaubatz, F. T. Hioe, and K. Bergmann, adiabatic population transfer in a three-level system driven by delayed laser pulses, *Phys. Rev. A* **40**, 6741 (1989).
- [21] B. Shore, coherent manipulations of atoms using laser light, *Acta Phys. Slovaca* **58**, 243 (2008).
- [22] D. Guéry-Odelin, A. Ruschhaupt, A. Kiely, E. Torrontegui, S. Martínez-Garaot, and J. G. Muga, shortcuts to adiabaticity: Concepts, methods, and applications, *Rev. Mod. Phys.* **91**, 045001 (2019).
- [23] R. Unanyan, L. Yatsenko, K. Bergmann, and B. Shore, laser-induced adiabatic atomic reorientation with control of diabatic losses, *Opt. Commun.* **139**, 48 (1997).
- [24] M. Demirplak and S. A. Rice, Adiabatic population transfer with control fields, *J. Phys. Chem. A* **107**, 9937 (2003).
- [25] M. Demirplak and S. Rice, On the consistency, extremal, and global properties of counterdiabatic fields, *J. Chem. Phys.* **129**, 154111 (2008).
- [26] M. V. Berry, Transitionless quantum driving, *J. Phys. A: Math. Theor.* **42**, 365303 (2009).
- [27] X. Chen, I. Lizuain, A. Ruschhaupt, D. Guéry-Odelin, and J. G. Muga, Shortcut to Adiabatic Passage in Two- and Three-Level Atoms, *Phys. Rev. Lett.* **105**, 123003 (2010).
- [28] Y.-X. Du, Z.-T. Liang, Y.-C. Li, X.-X. Yue, Q.-X. Lv, W. Huang, X. Chen, H. Yan, and S.-L. Zhu, Shortcut to adiabatic passage in two- and three-level atoms, *Nat. Commun.* **7**, 12479 (2016).
- [29] S. An, D. Lv, A. del Campo, and K. Kim, shortcuts to adiabaticity by counterdiabatic driving for trapped-ion displacement in phase space, *Nat. Commun.* **7**, 12999 (2016).
- [30] A. Vepsäläinen, S. Danilin, and G. S. Paraoanu, Superadiabatic population transfer in a three-level superconducting circuit, *Sci. Adv.* **5**, eaau5999 (2019).
- [31] Z. Yang, X. Tan, Y. Dong, X. Yang, S. Song, Z. Han, J. Chu, Z. Li, D. Lan, H. Yu, and Y. Yu, Realization of arbitrary state-transfer via superadiabatic passages in a superconducting circuit, *Appl. Phys. Lett.* **115**, 072603 (2019).
- [32] B. B. Zhou, A. Baksic, H. Ribeiro, C. G. Yale, F. J. Heremans, P. C. Jerger, A. Auer, G. Burkard, A. A. Clerk, and D. D. Awschalom, Accelerated quantum control using superadiabatic dynamics in a solid-state lambda system, *Nat. Phys.* **13**, 330 (2016).
- [33] A. Baksic, H. Ribeiro, and A. A. Clerk, Speeding up Adiabatic Quantum State Transfer by Using Dressed States, *Phys. Rev. Lett.* **116**, 230503 (2016).
- [34] X. Chen and J. G. Muga, Engineering of fast population transfer in three-level systems, *Phys. Rev. A* **86**, 033405 (2012).
- [35] X. Laforgue, X. Chen, and S. Guérin, robust stimulated Raman exact passage using shaped pulses, *Phys. Rev. A* **100**, 023415 (2019).
- [36] T.-N. Xu, K. Liu, X. Chen, and S. Guérin, Invariant-based optimal composite stimulated Raman exact passage, *J. Phys. B: At. Mol. Opt. Phys.* **52**, 235501 (2019).
- [37] A. Emmanouilidou, X.-G. Zhao, P. Ao, and Q. Niu, Steering an Eigenstate to a Destination, *Phys. Rev. Lett.* **85**, 1626 (2000).
- [38] V. Dorier, M. Gevorgyan, A. Ishkhanyan, C. Leroy, H. R. Jauslin, and S. Guérin, Nonlinear Stimulated Raman Exact Passage by Resonance-Locked Inverse Engineering, *Phys. Rev. Lett.* **119**, 243902 (2017).
- [39] J.-J. Zhu, X. Chen, H.-R. Jauslin, and S. Guérin, Robust control of unstable nonlinear quantum systems, *Phys. Rev. A* **102**, 052203 (2020).
- [40] B.-J. Liu and M.-H. Yung, Coherent control with user-defined passage, *Quantum Sci. Technol.* **6**, 025002 (2021).
- [41] N. V. Vitanov, A. A. Rangelov, B. W. Shore, and K. Bergmann, Stimulated Raman adiabatic passage in physics, chemistry, and beyond, *Rev. Mod. Phys.* **89**, 015006 (2017).
- [42] B. Broers, H. B. van Linden van den Heuvell, and L. D. Noordam, Efficient Population Transfer in a Three-Level Ladder System by Frequency-Swept Ultrashort Laser Pulses, *Phys. Rev. Lett.* **69**, 2062 (1992).
- [43] G. S. Vasilev, A. Kuhn, and N. V. Vitanov, Optimum pulse shapes for stimulated Raman adiabatic passage, *Phys. Rev. A* **80**, 013417 (2009).
- [44] J. P. Davis and P. Pechukas, Nonadiabatic transitions induced by a time-dependent Hamiltonian in the semiclassical/adiabatic limit: The two-state case, *J. Chem. Phys.* **64**, 3129 (1976).
- [45] F. Motzoi, J. M. Gambetta, P. Rebentrost, and F. K. Wilhelm, Simple Pulses for Elimination of Leakage in Weakly Nonlinear Qubits, *Phys. Rev. Lett.* **103**, 110501 (2009).
- [46] J. M. Gambetta, F. Motzoi, S. T. Merkel, and F. K. Wilhelm, Analytic control methods for high-fidelity unitary operations in a weakly nonlinear oscillator, *Phys. Rev. A* **83**, 012308 (2011).
- [47] Z. Chen, J. Kelly, C. Quintana, R. Barends, B. Campbell, Y. Chen, B. Chiaro, A. Dunsworth, A. G. Fowler, E. Lucero, E. Jeffrey, A. Megrant, J. Mutus, M. Neeley, C. Neill, P. J. J. O'Malley, P. Roushan, D. Sank, A. Vainsencher, J. Wenner, T. C. White, A. N. Korotkov, and J. M. Martinis, Measuring and Suppressing Quantum State Leakage in a Superconducting Qubit, *Phys. Rev. Lett.* **116**, 020501 (2016).
- [48] H. Ribeiro, A. Baksic, and A. A. Clerk, Systematic Magnus-Based Approach for Suppressing Leakage and Nonadiabatic Errors in Quantum Dynamics, *Phys. Rev. X* **7**, 011021 (2017).
- [49] R. Barends, *et al.*, Superconducting quantum circuits at the surface code threshold for fault tolerance, *Nature* **508**, 500 (2014).
- [50] M. Christandl, N. Datta, A. Ekert, and A. J. Landahl, Perfect State Transfer in Quantum Spin Networks, *Phys. Rev. Lett.* **92**, 187902 (2004).
- [51] X. Li, Y. Ma, J. Han, T. Chen, Y. Xu, W. Cai, H. Wang, Y. Song, Z.-Y. Xue, Z.-q. Yin, and L. Sun, Perfect Quantum State Transfer in a Superconducting Qubit Chain with Parametrically Tunable Couplings, *Phys. Rev. Appl.* **10**, 054009 (2018).
- [52] M. D. Reed, L. DiCarlo, B. R. Johnson, L. Sun, D. I. Schuster, L. Frunzio, and R. J. Schoelkopf, High-Fidelity Readout in Circuit Quantum Electrodynamics Using the Jaynes-Cummings Nonlinearity, *Phys. Rev. Lett.* **105**, 173601 (2010).
- [53] D. Sank, *et al.*, Measurement-Induced State Transitions in a Superconducting Qubit: Beyond the Rotating Wave Approximation, *Phys. Rev. Lett.* **117**, 190503 (2016).